Influence of the stress level and hygrothermal conditions on the creep/recovery behaviour of high-grade flax and hemp fibre reinforced GreenPoxy matrix composites

Authors: Benjamin Sala*, Xavier Gabrion, Frédérique Trivaudey, Violaine Guicheret-Retel, Vincent Placet

Affiliation : Univ. Bourgogne Franche-Comté, FEMTO-ST Institute, UFC/CNRS/ENSMM/UTBM, Department of Applied Mechanics, F-25000 Besançon.

Abstract: This paper investigates the influence of the stress level and hygrothermal conditions on the creep/recovery behaviour of three high-grade composites made of GreenPoxy and flax and hemp fibres. The results show that the levels of instantaneous, time-delayed and residual strains increase with the applied load and the severity of the environment. The time-delayed strains of the materials are higher in the creep phase than in the recovery phase. A stiffening effect is also observed during the recovery phase. The post-creep viscoelastic properties are then identified using an anisotropic viscoelastic law from the recovery function. The relaxation time function is independent of the stress level and the environmental conditions. The viscous parameter varies with the stress level and increases substantially with severe environmental conditions. The dependence of the creep/recovery behaviour on the stress level is due to the dependence of the stiffening phenomenon and irreversible mechanisms rather than to the viscoelastic behaviour.

Keywords: A. Biocomposite; B. Environmental degradation; B. Mechanical properties; D. Creep

1. INTRODUCTION

In the last two decades, plant fibres have emerged as an alternative to synthetic fibres, and the use of plant fibre composites (PFCs) has become a market reality [1–4], particularly in the transport sector [5,6]. Unfortunately, due to the lack of knowledge about their durability and behaviour under complex mechanical loading, they are not effectively used in structural applications. To date, the monotonic tensile behaviour of plant fibre composites has been substantially studied [7–9], and the literature reports physical-based models that are able to finely reproduce the experimentally observed behaviour [10–12]. However, the hygrothermal effect is not yet satisfactorily implemented in these predictive tools. Indeed, contrary to most petrosourced composites, PFCs are highly sensitive to hygrothermal conditions and their variation and/or cycling over time [13]. Their monotonic, fatigue and vibrational behaviours are reported to be significantly influenced by such parameters [8,9,14–19]. Complex behaviour is observed, including nonlinearities as well as strain hardening and strain-softening effects, depending on the mechanical loading and hygrothermal exposition combinations [9,17]. In contrast, the time-delayed behaviour has not been adequately investigated. This knowledge is, however, essential for ensuring a reliable design in various field applications. While the creep behaviour of short fibre composites is quite well

documented [20–24], unfortunately, the number of scientific articles focused on the creep behaviour of long fibre composites is limited [12,25–29]. However, plant fibres, such as hemp and flax, exhibit pronounced viscoelastic behaviour, even in the longitudinal direction [30,31]. This is a notable difference from carbon and glass fibres, which exhibit pure elastic behaviour in their axial direction. For hemp fibres, an increase in the time-delayed strain is also observed with increasing moisture content and under cyclic humidity [32]. To the best of the author's knowledge, at the scale of PFCs, creep behaviour is mainly studied under ambient environments. Poilâne *et al.* [25] investigated the influence of the stress level on the creep behaviour of flax/epoxy composites. They discovered a link between the time-delayed behaviour and the tensile monotonic biphasic behaviour. They also observed the existence of residual strains when the applied stress was greater than the yield point. They successfully described this complex behaviour, including irreversible phenomena, using a viscoelastoplastic model. The stiffening effect was also recently implemented in an updated version of this model [12]. More recently, Stochioiu *et al.* [26] modelled the viscoelastic behaviour of flax fibre laminates ([45/-45] layup) using Zenner and Burger models. They showed that these models are only able to describe the viscoelastic behaviour for low stress levels. None of the abovementioned studies take into account the influence of environmental conditions on time-delayed behaviour. The effect of temperature on the time-delayed behaviour of two flax fibre-reinforced PLA matrix composites and a jute fibre-reinforced PLA matrix composites was studied by Morreale *et al.* [27]. They noticed an increase in the time-delayed strain with increasing temperature. Durante *et al.* [28] studied the flexural creep behaviour of PLA matrix composite reinforced with woven hemp fabric at different values of temperature and with different fibre volume fractions. They showed that the long-term behaviour can be accurately predicted using the Time-Temperature Superposition principle for fibre volume fractions lower than 30%. Abida *et al.* [29] studied the creep behaviour of PFCs conditioned at different moisture contents using an aqueous saturated saline solution. The tests were performed under ambient conditions. The results showed an increase in the total and residual strains with increasing moisture content. In this paper, the authors showed that the time-delayed behaviour can be described with a viscoelastic-viscoplastic model only for low and moderate relative humidity (RH) values.

The present paper aims to fill the gap in the literature and studies the time-delayed behaviour of PFCs under severe environments. Creep/recovery tests under tensile loading are performed at various stress levels in contrasting environments: ambient conditions (23°C, 50% RH) and severe environment (70°C, 85% RH). Flax and hemp fibre reinforced GreenPoxy matrix composites are tested. For the flax fibres, tape is used to manufacture unidirectional (UD) and cross-ply (CP) laminates. For the hemp fibres, a woven fabric is used. These reinforcement materials are currently the front-runner for the production of structural PFCs. The creep/recovery response is thoroughly analysed, and the instantaneous, time-delayed and irreversible strains are

quantified. A continuum spectrum 3D-viscoelastic model that was previously developed for anisotropic materials [33] is then updated and used to identify the post-creep viscoelastic properties of the tested materials and characterize the influence of the stress and environmental parameters.

2. MATERIALS AND METHODS

2.1. Specimen preparation

2.1.1. Reinforcements and matrix

Two types of reinforcement materials were used in this work: a unidirectional flax tape with an areal weight of 110 g/m^2 (L-FlaxTape-110-36) manufactured by LINEO® and a hemp woven fabric produced by Linificio e Canapificio Nazionale. For the hemp reinforcement, the fabric, with an average areal weight of 350 g/m^2, was made from hemp rovings weaved following a satin 6 effect diagram with a density of 6.5 yarns/cm in each direction, as described in [34]. The epoxy system, used for both reinforcements, was composed of a partially biosourced epoxy resin containing 56% carbon from plant origin (GreenPoxy 56) and its hardener (SD 7561). Both the resin and hardener were provided by SICOMIN®.

2.1.2. Composite manufacturing

Composite plates were produced using hand lay-up and impregnation and a thermocompression process. FlaxTape plies were laid up forming unidirectional and cross-ply laminates, denoted FUD and FCP, respectively. Hemp woven fabrics were also stacked to produce the woven fabric composites denoted HWF. A symmetric lay-up was employed for both the FCP and HWF composites. The number of plies in the laminates was optimized to obtain a composite thickness that was well suited for the characterization methods. The stacking sequences of the manufactured plates are described in Tab. 1. Before composite production, all the plies were dried at 60°C for 24 h. As the sorption phenomena in the thin plies of FlaxTape are extremely fast, it was observed that the fibre regained a significant amount of moisture during the lay-up and impregnation steps. The process was slower for the hemp woven fabrics, which have higher thicknesses and areal weights. The matrix was mixed with the hardener at a ratio of 0.37. The plies were impregnated with an excess of matrix in the steel mould with dimensions of 300x200 mm². The metallic parts were previously covered by Teflon to avoid getting adhesion from the resin on the mould. The FlaxTape plies were impregnated following a specific protocol, described in [7], to optimize their impregnation while limiting fibre waviness and disorientation. A strip of resin was poured in the centre of each ply perpendicular to the fibre direction. With the application of pressure, the matrix flowed towards the fibre length. The hemp fabric plies were covered with resin using a roller to facilitate impregnation. The mould was then closed only at two of its four lateral sides to allow the excess matrix and trapped air to escape when applying pressure, as described in [18]. The mould was placed between the platens of the AGILA®

Presse 100 kN thermocompression machine to undergo the curing cycle. As soon as the mould reached a temperature of 40°C, a pressure of 3 bar was applied. After 15 minutes at this temperature, the mould was heated again to reach the curing temperature Tc, which was maintained for 1 hour. The heating was then turned off, and the composite plate temperature decreased. The pressure was released at the temperature Tpr. Post-curing at temperature Tpc for a duration dpc was carried out within 2 days. The values of the temperature and time parameters are all summarized in Tab. 2. The curing protocols were optimized during the preliminary tests to ensure the full curing of the epoxy system. The average volume ratios of the fibres (Vf) and voids (Vv) were then determined using the procedure adapted from ASTM D 3171-99 [35]. These data are available Tab. 2.

2.1.3. Sample preparation

The plates were laser cut using a Trotec Speedy 300® laser device to avoid the use of any water or lubrication. The FUD samples were cut in the fibre direction (L direction) and transverse direction (T direction). The HWF composite specimens were cut following the weft direction. The dimensions of the composite samples are given in Tab. 1. Some of the cut specimens were used for mechanical testing (see section 2.2), and others were used for the determination of the equilibrium moisture content (EMC) in the different testing environments (see section 2.1.5)

For the mechanical tests performed at 70°C – 85% RH, aluminium end tabs were glued on the extremities of the samples. The preliminary tests showed slippage and premature failure in these areas. Both the aluminium and the composite were previously sanded and cleaned with acetone. The end tabs were then bonded using a bicomponent epoxy adhesive (Loctite EA 9492).

2.1.4. Conditioning

The samples were stored in an environmental chamber. A first batch of specimens was stored in a climatic chamber Memmert HPP 108 L at 23°C and 50% RH, named environmental condition (EC1). A second batch was conditioned in a climatic chamber Climats® Excal 1411-HA at 70°C - 85% RH, named environmental condition 2 (EC2). They were stored for 20 days and 10 days to ensure that they reached moisture content equilibrium.

2.1.5. Determination of the moisture content at equilibrium

The moisture contents at equilibrium for the EC1 and EC2 environments, denoted EMC^{EC1} and EMC^{EC2}, were measured for each type of laminate using at least 4 samples. The specimens were first stored under environmental condition EC1. Once hygroscopic equilibrium was reached, the weight of the sample ${m_\infty}^{EC1}$ was measured with a balance with an accuracy of 0.001 g. The anhydrous mass m_{anh} was similarly determined by

drying the specimens in an oven at 103°C. Finally, the samples were stored under environmental condition EC2, and the specimens were weighed after they reached equilibrium. This mass was denoted ${m_\infty}^{EC1}$.

The moisture content at equilibrium EMC^{ECi} corresponding to environmental condition ECi was calculated using the following equation described in ASTM D 5229-92 [36]:

$$EMC^{ECi} = 100 \times \frac{{m_\infty}^{ECi} - m_{anh}}{m_{anh}}, \quad (1)$$

2.2. Mechanical testing

2.2.1. Monotonic tensile tests

An MTS Criterion 45 machine was used to determine the monotonic properties of composites under tensile loading. A 100 kN load cell was installed on the machine when the FUD composite was tested. A 5 kN cell was used for testing the HWF and FCP composite. The crosshead speed was set at 1 $mm.s^{-1}$ in accordance with ASTM D 3039/D 3039M-17 [37]. For samples tested under environmental condition EC2, a climatic chamber Inec-70/90 from Ineltec® was installed on the machine to control the relative humidity and the temperature surrounding the specimen to maintain the EMC. The mechanical test under environmental condition EC1 was realized at room temperature. The temperature and RH in the air surrounding the specimens were recorded during the tests. The average values were 23°C ± 3° and 50% ± 10% RH, respectively. All samples were instrumented with an Instron® 2620-601 contact extensometer with a 50 mm gauge length and a measuring range of ± 10%. The stress was calculated as the ratio of the measured force to the initial cross section. The tensile response of a PFC tested in the fibre direction is not linear and is qualified as a biphasic behaviour [38]. Therefore, two apparent moduli, E_L^1 and E_L^2, were calculated in each phase using linear regression in the ranges between 0.01% - 0.15% strain and from 0.4% strain until failure. The mean mechanical properties were calculated using at least 4 samples. The confidence interval was taken as being equal to the standard deviation. For the sake of clarity, only one representative strain/stress curve of each tested material is generally plotted or presented in the paper.

2.2.2. Creep tensile tests

Creep tests were carried out on the same machine instrumented with the same load cells. The load path was comprised of a one-hour creep phase followed by a recovery phase of the same duration. During the tests, the hygrothermal conditions were controlled using the same devices and protocols that were used for the monotonic tensile tests. The temperature and RH of the air surrounding the specimen were systematically recorded during the tests using a sensor placed either in the climatic chamber or in the room. The dimensions of the samples were the same as those described for the monotonic tensile test and were dependent on the environmental conditions

of the test (see Tab. 1). In accordance with ISO 899-1 [39], the nominal stress, σ_{nom}, was reached between 1 and 5 seconds. The loading and unloading speeds were equal. The samples were also instrumented with a contact extensometer. Three samples were tested per stress level. Each curve represented the result obtained for one specimen.

The following mechanical characteristics were extracted from the creep/recovery response:

- the instantaneous strain determined during the loading ε_{ins}^{c} and corresponding to the total strain once the nominal stress was reached,
- the maximum strain ε_{max} measured at the end of the creep stage, i.e. at the time 3600s,
- the maximum time-delayed strain value ε_{del}^{c} determined during the creep stage and defined as the difference between ε_{max} and ε_{ins}^{c},
- the time at the beginning of the recovery stage t_0,
- the instantaneous strain determined during the unloading ε_{ins}^{r} corresponding to the difference between ε_{max} and $\varepsilon(t_0)$ the total strain at time t_0,
- the time-delayed strain ε_{del}^{r} corresponding to the maximum time-delayed strain measured during the recovery stage and defined as the difference between ε_{res} and $\varepsilon(t_0)$,
- the residual strain ε_{res} measured at 7200s,
- the strain rate during the secondary creep stage $\dot{\varepsilon}_{creep}$ measured by averaging the strain rates calculated every minute on the time range 2000-3500 sec,
- the tangent modulus ${E_{tang}}^{load}$ determined during the loading step of the creep/recovery test by a linear regression in the range 0.01%-0.15% of strain,
- the tangent modulus ${E_{tang}}^{unload}$ determined during the unloading step of the creep/recovery test by a linear regression in the range $\varepsilon_{max} - 0.01\%$ strain and $\varepsilon_{max} - 0.15\%$ of strain.

They are described in Fig. 1. The parameter S, described by the following equation, allows the stiffening phenomenon that may occur during unloading to be estimated:

$$S = 100 \times \frac{{E_{tang}}^{unload} - {E_{tang}}^{load}}{{E_{tang}}^{load}}, \quad (2)$$

2.3. Identification of the viscoelastic properties

2.3.1. Viscoelastic model

The deformation behaviour in the creep function results not only from the viscoelastic behaviour but also from other phenomena associated with the observed stiffening and residual strains. Taking into account this aspect, it appeared more relevant to use the recovery phase, free of the stiffening phenomena, to catch the viscoelastic

behaviour only. The material behaviour being undeniably affected by the previous loading phase [40], the properties identified using the recovery phase will refer to the post-creep viscoelastic behaviour.

An anisotropic constitutive law was used to identify the post-creep viscoelastic properties. It was adapted from the formulation proposed by Boubakar *et al.* [33]. The viscoelastic flow is defined by a second order tensor $\underline{\varepsilon^{ve}}$ as a sum of N second order tensors $\underline{\xi_i}$ corresponding to the elementary mechanisms of viscoelastic flow.

The evolution law of the viscoelastic flow is given by the following equation:

$$\underline{\dot{\varepsilon}}^{ve} = \sum_{i=1}^{N} \underline{\dot{\xi}_i} = \sum_{i=1}^{N} \frac{1}{\tau_i} (\mu_i \underline{\underline{S_{ve}}}\,\underline{\sigma} - \underline{\xi_i}), \tag{3}$$

where $\tau_i$and μ_i are the release time and the weighting coefficient of the ith elementary viscous mechanism, respectively; $\underline{\underline{S_{ve}}}$ is the viscoelastic compliance tensor; $\underline{\sigma}$ is the Cauchy true stress tensor; and N is the number of elementary viscous mechanisms.

The expression of the viscoelastic compliance $\underline{\underline{S_{ve}}}$ was modified from the original formulation written for glass fibre composites. Contrary to the behaviour of synthetic fibres, plant fibres exhibit viscoelastic behaviour in their longitudinal direction. Thus, the term in the first column and the first row of the viscoelastic compliance tensor was added (instead of the null value in the initial formulation) to take into account the potential time-dependent behaviour of the composites in the fibre direction.

$$\underline{\underline{S_{ve}}} = \begin{bmatrix} \frac{\beta_L}{E_L} & -\beta_{LL}\frac{\nu_{LT}}{E_L} & -\beta_{LL}\frac{\nu_{LT}}{E_L} & 0 & 0 & 0 \\ -\beta_{LL}\frac{\nu_{TL}}{E_L} & \frac{\beta_T}{E_T} & -\beta_{TT}\frac{\nu_{TT}}{E_T} & 0 & 0 & 0 \\ -\beta_{LL}\frac{\nu_{TL}}{E_L} & -\beta_{TT}\frac{\nu_{TT}}{E_T} & \frac{\beta_T}{E_T} & 0 & 0 & 0 \\ 0 & 0 & 0 & \frac{\beta_{LT}}{G_{LT}} & 0 & 0 \\ 0 & 0 & 0 & 0 & \frac{\beta_{LT}}{G_{LT}} & 0 \\ 0 & 0 & 0 & 0 & 0 & \frac{\beta^*}{G_{TT}} \end{bmatrix}$$

$$\text{with } \frac{\beta^*}{G_{TT}} = 2\left(\frac{\beta_T}{E_T} + \frac{\beta_{TT}\nu_{TT}}{E_T}\right), \tag{4}$$

where $\beta_L, \beta_T, \beta_{LL}, \beta_{TT}, \beta_{LT}, \ and\ \beta^*$ are the six viscoelastic material parameters that characterize the material viscosity; E_i is the elastic moduli corresponding to each material direction, while $\nu_{ij}\ and\ G_{ii}$ is the poison ratio and shear moduli in plan (i,j).

In this generalized viscoelastic model and to maintain physical meaning, we have considered that the rigidities respect a defined distribution as a function of the logarithm of the relaxation time. A Gaussian function was used in the present work to represent the distribution of μ_i as a function of the logarithm of the release time ($\ln(\tau_i)$).

This distribution is described by the mean $\ln(\tau_1)$ and the standard deviation SD. The Gaussian spectrum was already used to model the creep behaviour of single plant fibres [30].

This model is well suited for the description of the viscoelastic behaviour of such PFCs, as illustrated in Fig. 1 c).

2.3.2. Identification of model parameters

In this study, unidirectional creep/recovery loading was applied to the composite samples. For this analysis, the only parameter of the viscoelastic compliance tensor involved in the time-delayed strain response was $\frac{\beta_L}{E_L}$. This parameter as well as $\ln(\tau_1)$ and SD were identified by the inverse method.

The identification process was carried out on the recovery function, which was defined as the ratio of the time-delayed strain during the recovery stage $\varepsilon^r(t)$ and the nominal stress. The time-delayed strain $\varepsilon^r(t)$ was extracted from the creep/recovery test as presented in Fig. 1 b) and was defined by the following equation:

$$\varepsilon^r(t), = \varepsilon(t_0) - \varepsilon(t), \forall t \geq t_0, \quad (5)$$

The viscous parameter β_L was determined for each sample by multiplying the identified value of $\frac{\beta_L}{E_L}$ by the modulus determined during unloading of the creep/recovery test ${E_{tang}}^{unload}$.

The identification of the model parameters was performed using a hybrid optimization algorithm. This tool avoided convergence towards local optima in the case of multimodal test functions. It combines a heuristic method based on a genetic algorithm and the Levenberg-Marquardt algorithm, both of which are implemented in the free access code MIC2M, which is well suited for finding local minima.

3. RESULTS AND DISCUSSION

3.1. Monotonic tensile behaviour under ambient conditions

The monotonic behaviours of the FUD, HWF and FCP composites are first studied under ambient conditions (EC1). Fig. 2 presents the tensile stress-strain curves of these composites as well as the evolution of the tangent modulus as a function of the applied stress. The FUD composite in the L direction and the FCP composite exhibit the typical biphasic behaviour observed for PFCs [8] (see Fig. 2 a). In the first phase, the material behaviour is quasi linear until the yield point, located at approximately 55 MPa for the FUD composite and approximately 35 MPa for the FCP composite. The second phase starts beyond this threshold. The tangent modulus decreases suddenly to reach an almost constant value (see Fig. 2 b). The mechanical response of the FUD composite solicited in the T direction is almost perfectly linear. The determined tensile properties are summarized in Tab. 3. The values of the initial tangent modulus of the FUD composite according to directions L and T are equal to 36 GPa and 4.2 GPa, respectively. Their mean strengths are 311 MPa and 16 MPa,

respectively. These values are in agreement with the data from the literature and the supplier datasheet [16,41]. For the cross-ply laminate, the initial tangent modulus is equal to 17 GPa, and the strength is 177 MPa on average. Very similar values are obtained for the hemp woven fabric composite (which has a slightly higher Vf than that of the FCP specimens), with a mean initial tangent modulus and strength equal to 19 GPa and 176 MPa. In contrast, a significant difference in the strain at failure is observed, with 1.3% for the FCP composite and 1.74% for the HWF composite. The non-linear behaviour of the HWF composite is very similar to classical elastoplastic behaviour. This difference is attributed to the architecture of the reinforcement. Beyond the difference in the type of fibres (flax and hemp), the two composites have two different fibre architectures (non-crimp fabric and woven fabric). In the woven fabric, the fibre disorientation (resulting from the twist in the rovings and crimp) provides more deformability of the composite when loaded in the main material direction.

3.2. Influence of the stress level on the creep/recovery behaviour under ambient conditions

Creep/recovery behaviour

The time-delayed behaviour of the composites is then studied under ambient conditions and for various stress levels between 15 MPa and 150 MPa. Indeed, the question of the linearity of the viscoelastic behaviour of the PFCs is still unsolved in the literature. The evolution of the strain behaviour during the creep/recovery tests is presented in Fig. 3. When the load is applied almost instantaneously, a rapid increase in the strain is observed (ε_{ins}^{c}). As a function of time, the strain rate decreases from high values in the primary creep stage to a lower and almost constant value $\dot{\varepsilon}_{creep}$ in the secondary creep stage. The time-delayed (ε_{del}^{c}) and total strains (ε_{max}) then evolve over time to reach their maximum values at the end of the creep stage. During the unloading stage, an instantaneous strain decrease is initially observed (ε_{ins}^{r}). The strain then evolves over time (ε_{del}^{r}) with an initially rapid rate and then slows down. A residual strain is then observed at the end of the test (ε_{res}) for most of the testing conditions. All the values measured for these properties are presented in Tab. 4, Tab. 5 and Tab. 6 for the FUD, HWF and FCP composites, respectively.

- FUD composite

The results obtained for the FUD composite are presented in Fig. 3 a) and Tab. 4. It can be observed that the level of maximum strain ε_{max} increases with the applied load from 0.05 % at a nominal stress of 15 MPa to 0.68 % at 150 MPa. The secondary creep strain rate $\dot{\varepsilon}_{creep}$ increases with the stress level from 0.5 s^{-1} at 25 MPa to 6.3 s^{-1} at 100 MPa. During the creep stage, the time-delayed strain ε_{del}^{c} also increases with the applied load and represents 17 % and 20 % of the instantaneous strains ε_{ins}^{c}, respectively. The time-delayed strain measured during the recovery stage ε_{del}^{r} is lower than that obtained during the creep stage. This difference is equal to 26 %

for a nominal stress of 150 MPa. This is explained by the presence of residual strains ε_{res} after unloading, even after 3600 s. For nominal stresses lower than the yield point (approximately 55 MPa), the initial length of the specimens is recovered after 1000 s, and no residual strains are observed. Beyond this stress level, the residual strains after 3600 s of recovery increase with increasing stresses, reaching values of 0.04 % and 0.13 % for 70 MPa and 150 MPa, respectively. These results are in agreement with the works of Poilâne *et al.* [25], pointing out the appearance of residual strains after creep/recovery testing only for stress levels higher than the yield point.

The results of the present study also show that the stiffening phenomena in the creep/recovery test are also observed for stress levels higher than the yield point. Particularly, at 150 MPa, the level of instantaneous strain during the unload stage ε_{ins}^{r} is 11 % lower than during the loading stage ε_{ins}^{c}. The stiffening coefficient is null for the stress level below the yield point and increases with increasing stress levels higher than this threshold. The stiffening coefficient ranges from 1.4 % to almost 10 % for stress levels varying from 70 MPa and 150 MPa. This behaviour is very similar to that observed at the scale of single plant fibres such hemp [30,32]. The authors attributed the observed stiffening phenomena and residual strains observed for loading beyond a threshold value to a stick-slip mechanism of cellulose microfibrils within the fibre wall [42]. In pure UD PFCS, such as FUD, the observed behaviour at the scale of the composite could result from the specific behaviour of the plant fibre themselves. The modelling of the whole creep/recovery behaviour of FUD would require constitutive laws integrating such mechanisms. To date, this type of behaviour has been described only using viscoelastic-viscoplastic models [12,25,29], which are able to reproduce the observed behaviour but do not rely on physics.

- FCP composite

The time-delayed behaviour of the FCP composite is presented in Fig. 3 b), and the associated mechanical properties are summarized in Tab. 5. As for the FUD composite, the maximum strain increases with the stress level from 0.14% at 25 MPa to a value of 0.84% at 100 MPa. During the secondary creep stage, the strain evolves at a higher speed for the case of the FCP composite than for the FUD composite, with an average difference of approximately 2 s^{-1}. The time-delayed strain measured during the creep stage, ε_{del}^{c}, is an increasing function of the loading level and represents 20% of ε_{ins}^{c}. The level of time-delayed strain during the recovery stage reaches values from 0.018% to 0.10%, and, as for the FUD composite, is lower than ε_{del}^{c}.

It can be observed that the level of residual strain and the stiffening coefficient increase gradually as soon as the applied stress is above the yield point (approximately 35 MPa) and finally reach a value of 0.14% and 6.5 % at 100 MPa, respectively. All these results highlight the presence of irreversible phenomena, as observed for FUD composite. However, the stiffening of the FCP composite appears to be lower than that of the FUD composite. For the FCP composite solicited at 100 MPa, corresponding to 56% of the ultimate tensile stress, the stiffening

coefficient is equal to 6.5%. In comparison, the stiffening of the FUD composite is estimated at 10% for a stress level at 150 MPa, corresponding to 48% of the ultimate tensile stress. It is also important to emphasize that the S coefficient is greater at 70 MPa than at 100 MPa with a value of 7.6%. In addition, the coefficient of variation of parameter S for the stress level at 100 MPa is approximately 115%. All these results can be explained by the competition between the stiffening and damage mechanisms inside the composite.

- HWF composite

The results related to the HWF composite are presented in Fig. 3 c) and Tab. 6. Except for the higher stress level, the values of the maximum strain of the HWF composites are relatively close to that of the FCP composite, with a maximal strain difference not exceeding 8%. The similarity in the time-delayed behaviour can be explained by the almost identical tensile responses observed under monotonic testing over the stress range up to 80 MPa. For a higher stress level, the static behaviour differs from that of the FCP composite, and the maximum strain level of the HWF composite reaches a value of 1.15%, which is 40% higher than the maximum strain of the composite FCP.

During the creep stage, the measured strain rates and time-delayed strain of the HWF composite are two times higher than the values obtained for the FCP composite at a stress level of 100 MPa. The proportion of time-delayed strain in relation to the maximum strain and the instantaneous strain is of an order of magnitude of 20% and 30%, respectively. Even during the recovery stage, the level of the time-delayed strain of the HWF composite is similar to that of the FUD composite in the stress range from 0 MPa to 80 MPa but then becomes 73% higher at a stress level of 100 MPa. All these results show that the delayed mechanical response of the composite reinforced by a woven fabric is more important both in amplitude and speed. This can be explained by the appearance of additional strain caused by the disorientation of the fibres due to twisting and shrinkage during the weaving process. Irreversible mechanisms are also expressed in the HWF composite by the appearance of residual strain for a load greater than 35 MPa. The level of residual strain is almost identical in the HWF and FCP materials for the stress range between 25 MPa and 70 MPa. The stiffening phenomena appearing in the HWF composite for stress levels greater than 35 MPa are more preponderant in the FCP composite, with a maximum difference in the S parameter being approximately 77% higher than that of the HWF composite.

Post-creep viscoelastic properties

The post-creep viscoelastic behaviours of the three composites are also specifically studied by using the recovery function and the anisotropic model. The recovery function is studied instead of the creep function to leave out the strain behaviour resulting from the stiffening as well as the residual strains. It is thus considered that the recovery curve is free from stiffening effect. The identified parameters for the FUD, HWF and FCP composites are summarized in Tab. 7. The continuum spectra, linking the weighting coefficients and the release times, are

identified for each composite type and each stress level and are plotted in Fig. 4. It can be observed that all the spectrum distributions of the relaxation times are very similar, regardless of the stress level. This clearly indicates that the release time is independent of the stress level.

Fig. 5 presents the identified values of the viscous parameter β_L depending on the stress level and the composite type. The distribution of the values shows that they are all between 0.1 and 0.4. The viscous parameter tends to increase with the stress level, even if this trend is not respected at 70 MPa. For FUD and FCP composites, the value of β_L is higher at 70MPa than at the higher stress levels while this value is lower than the lower stress levels in the case of HWF composite. These observations therefore show, whatever the type of composite, a dependence of the viscous parameter on the stress level with a singularity at 70 MPa which needs to be investigated in the future.

3.3. Impact of severe environmental conditions

Monotonic tensile behaviour

The tensile behaviours of the three composites are also studied for the severe environmental condition EC2. The results are presented in Fig. 6 and Tab. 3. The moisture contents of the composites are available in Tab. 2. These values are approximately 5 points higher than the environmental condition EC1.

Fig. 6 a) shows the impact of these severe conditions on the stress-strain response under monotonic loading for the different materials. The evolution of the apparent modulus as a function of the stress is presented in Fig. 6 b). In contrast with the biphasic behaviour observed at ambient conditions, materials exhibit triphasic behaviour in severe environment.

The monotonic tensile behaviour is quasi-linear until the first yield point i1. This yield point is observed at relatively low stress levels, approximately 10 MPa for the FUD and FCP composites and approximately 25 MPa for the HWF composite. A significant decrease in the tangent modulus can be observed before yield point i1. Beyond this threshold, the behaviour is again quasi-linear until the yield point i2. Beyond i2, the tangent modulus increases gradually until failure. In particular, for the unidirectional composite, the apparent modulus decreases to a value of 10 GPa at yield point i1 to finally reach a value of approximately 20 GPa at the end of the test. This observed behaviour is similar to the type III behaviour observed at the fibre scale [42]. Due to the high temperature and moisture, the mobility of the polymer macromolecules is increased both in the matrix and in the fibre wall. This can explain why the fibre behaviour is more influential on the composite behaviour in severe conditions than in ambient conditions. In addition, it can be observed that the behaviour of the HWF composite is greatly affected by the change in environment and is explained by a greater displacement of the satin weave in the composite.

The tangent modulus E_L^1, the stress and the strain at failure are summarized in Tab. 3. When compared to ambient conditions, the initial stiffness is 64%, 74% and 59% lower for the FUD, HWF and FCP composites, respectively. The environmental conditions also influence the stress at failure with a decrease in the value of this parameter of approximately 30%. Conversely, with the severity of the environment, the strain at failure of the composites reinforced by flax fibres increases by approximately 20%, while the increase is approximately 79% for the hemp fibre composite.

Creep/recovery behaviour

Creep/recovery tests at different loading levels are also carried out for the environmental condition EC2 to estimate the impact of a severe environment on the time-delayed behaviour of the composites. The strain response of the materials is presented in Fig. 7. A cross at the end of the curves represent the failure of the samples. For a load level equal to approximately 75% of the average tensile strength, all the FUD samples failed (see Fig. 7 a)). Before failure, a tertiary creep stage can be seen for only one sample. The failure of the other specimens is more sudden. The initiation of failure occurs outside the gauge length of the extensometer, making it impossible to detect this sudden increase in strain. This breaking mode is also observable for only one sample of the FCP composite and HWF composite at approximately 55% and 60% of their average tensile strength, respectively and is explained by the variability of the stress at failure from one specimen to the other. Regardless of the type of material, the beginning of the tertiary creep stage appears for a strain of approximately 70% of the quasi-static strain at failure. One way to prevent material failure would therefore be to design structures based on their strain rather than their stress.

The values of the maximum and residual strains corresponding to the FUD, FCP and HWF composites are summarized in Tab. 8, Tab. 9 and Tab. 10, respectively. The results show a noticeable increase in these two values of strain for all the stress levels when compared to environment EC1. The maximum strain of the FUD and FCP composites is up to twice as high compared to those in EC1. Concerning the residual strain of these two composites, the value can be up to 6 times higher than those in EC1. The time-delayed behaviour of the HWF composite is more significantly impacted by changes in the environment. The maximum and residual strains can be approximately 4 times and 11 times higher than under condition EC1, respectively. The time-delayed strain of the FUD and HWF composites during the creep stage is on average 5 times higher under severe environmental conditions than under condition EC1. This parameter is only 1.7 times higher for the FCP composite. The time-delayed strain determined during creep is also higher than that determined during the recovery stage. For the case of the FUD composite at a stress level of 70 MPa, this difference is three times higher than that under ambient conditions and implies that there is a dependence of the irreversible phenomena on the change in environment.

A similar observation is made for the instantaneous strain during the loading step, which is on average three times higher for the FUD and HWF composites and only 1.9 times higher for the FCP composite than under ambient environment conditions. It can be assumed that the time-delayed behaviour is less influenced in the cross-ply composite due to a lower fibre volume fraction in the longitudinal direction than its counterparts. The level of time-delayed strain during the recovery stage of the FUD, FCP and HWF composites is also impacted with values 2.5, 2 and 3.5 times higher compared to those of environmental condition EC1, respectively.

Due to a low yield stress, stiffening in the composites occurs regardless of the studied load level. Moreover, the severity of the environment greatly increases this phenomenon. The S coefficient corresponding to the FUD, HWF and FCP composites reaches maximum values of 100%, 72% and 94%, respectively. The intensity of the stick slip mechanism therefore increases with the severity of the environment. The stiffening coefficient of the cross-ply composite is equal to 91% and 94%, and the confidence interval is evaluated at 18% and 1%, respectively, for a stress level of 55 MPa, corresponding to 43% of the tensile strength, and 70 MPa, corresponding to 55% of the tensile strength.

This substantial stiffening occurring at a stress level lower than the higher stress level reveals the presence of damage inside the cross-ply composite. The same observations can be observed for the HWF composite.

Post-creep viscoelastic properties

The values of the identified parameters and the associated continuum spectrum are presented in Tab. 7 and Fig. 8. The spectrum of the relaxation times relative for each stress level are superimposed for all the composites. This indicates that the environment does not influence the linearity of the time release with respect to the stress level. Fig. 9 presents the continuum spectrum determined for the FUD composite under the two studied environmental conditions. The superimposition of the spectrum clearly shows that the release times are independent of the environment, at least for the studied conditions.

The distribution of the values of the viscous parameter β_L for all the composites and stress levels are given in Fig. 10. Under a severe environment, the increase in the maximum value of this parameter is approximately 54%, 43% and 118% for the FUD, FCP and HWF composites, respectively, compared to those of the ambient conditions. The value of the viscous parameter is substantially impacted by changes in the environmental conditions. β_L is in the range of 0.6-0.85 for the HWF composite, while the values are between 0.2 and 0.4 for the FUD and FCP composites. Regarding the results obtained for the FUD composite, the viscous parameter is independent of the studied stress levels with a constant value of approximately 0.40. For the environmental condition EC1, it can be observed that the value of β_L changes depending on whether the stress level is below or above the yield point. The first yield point of the FUD composite is approximately 10 MPa for a more severe

environment. The change in the value of the viscous parameter is not observed for this environmental condition but supports the fact that β_L is constant for a stress level above the yield point for a unidirectional composite. A decrease in β_L is observed for the FCP and HWF composites with an increasing stress level. This is attributed to the increased viscous behaviour in the transverse direction expressed by the plies oriented at 90°.

4. CONCLUSIONS

The aim of this work was to contribute to the understanding of the time-delayed behaviour of plant fibre composites, particularly under in-service environmental conditions. The creep/recovery behaviour was investigated for a large range of stress and under two environmental conditions: 23°C-50% RH and 70°C-85% RH. Three types of composite materials, made with the current front-runner plant fibre reinforcements, were studied: flax unidirectional, flax cross-ply and hemp satin woven fabric reinforced Greenpoxy-based composites. The experimental results highlight a higher level of time-delayed strain during the creep stage than during the recovery stage. This is attributed to the simultaneous expression of the viscoelastic behaviour and of the stiffening effect which can rely on a stick slip phenomena at the fibre level. This mechanism is responsible for the occurrence of irreversible strains and a stiffening of the materials at a stress level above the yield stress. Moreover, the level of total and residual strain as well as the stiffening of the material increase with the stress level and the severity of the environment indicating the dependence of irreversible mechanisms on the environmental conditions and stress level.

The study of the post-creep viscoelastic behaviour also points out that the release time of the viscoelastic behaviour of the composites is independent of the environmental conditions and stress level, contrary to the viscous parameter.

Acknowledgements

The authors would like to acknowledge the funding received from the Bio Based Industries Joint Undertaking under the European Union's Horizon 2020 research and innovation program under grant agreement No 744349– SSUCHY project. The authors would also like to express special thanks to Gerard Michel and his team for their help in machining the samples by laser cutting. The authors thank the Company "Linificio e Canapificio Nazionale" from Italy for providing the hemp yarn and rovings used in this study.

REFERENCES

[1] CELC. Flax & Hemp Fiber composites, a market reality, the biobased solutions for the industry. JEC Group. 2018.

[2] Pil L, Bensadoun F, Pariset J, Verpoest I. Why are designers fascinated by flax and hemp fibre composites? Compos Part Appl Sci Manuf 2016;83:193–205.

[3] Bourmaud A, Beaugrand J, Shah DU, Placet V, Baley C. Towards the design of high-performance plant fibre composites. Prog Mater Sci 2018;97:347–408.

[4] Mohanty AK, Vivekanandhan S, Pin J-M, Misra M. Composites from renewable and sustainable resources: Challenges and innovations. Science 2018;362:536–42.

[5] Fogorasi M, Barbu I. The potential of natural fibres for automotive sector - review. IOP Conf Ser Mater Sci Eng 2017;252:012044.

[6] Mohammed L, Ansari MNM, Pua G, Jawaid M, Islam MS. A Review on Natural Fiber Reinforced Polymer Composite and Its Applications. Int J Polym Sci 2015;2015:1–15.

[7] Cadu T, Berges M, Sicot O, Person V, Piezel B, Van Schoors L, et al. What are the key parameters to produce a high-grade bio-based composite? Application to flax/epoxy UD laminates produced by thermocompression. Compos Part B Eng 2018;150:36–46.

[8] Berges M, Léger R, Placet V, Person V, Corn S, Gabrion X, et al. Influence of moisture uptake on the static, cyclic and dynamic behaviour of unidirectional flax fibre-reinforced epoxy laminates. Compos Part Appl Sci Manuf 2016;88:165–77.

[9] Réquilé S, Le Duigou A, Bourmaud A, Baley C. Hygroscopic and Mechanical Properties of Hemp Fibre Reinforced Biocomposites. Rev Compos Matér Avancés 2019;29:253–60.

[10] Mahboob Z, Chemisky Y, Meraghni F, Bougherara H. Mesoscale modelling of tensile response and damage evolution in natural fibre reinforced laminates. Compos Part B Eng 2017;119:168–83.

[11] Strohrmann K, Hajek M. Bilinear approach to tensile properties of flax composites in finite element analyses. J Mater Sci 2019;54:1409–21.

[12] Richard F, Poilâne C, Yang H, Gehring F, Renner E. A viscoelastoplastic stiffening model for plant fibre unidirectional reinforced composite behaviour under monotonic and cyclic tensile loading. Compos Sci Technol 2018;167:396–403.

[13] Assarar M, Scida D, El Mahi A, Poilâne C, Ayad R. Influence of water ageing on mechanical properties and damage events of two reinforced composite materials: Flax–fibres and glass–fibres. Mater Des 2011;32:788–95.

[14] Scida D, Assarar M, Poilâne C, Ayad R. Influence of hygrothermal ageing on the damage mechanisms of flax-fibre reinforced epoxy composite. Compos Part B Eng 2013;48:51–8.

[15] Abida M, Gehring F, Mars J, Vivet A, Dammak F, Haddar M. Effect of hygroscopy on non-impregnated quasi-unidirectional flax reinforcement behaviour. Ind Crops Prod 2019;128:315–22.

[16] Cadu T. Contribution au développement de l'utilisation des fibres naturelles dans les composites structuraux. Étude du comportement d'un composite Lin/Epoxy lors d'un vieillissement hygrothermique. Université de Bourgogne, 2018.

[17] Jeannin T, Berges M, Gabrion X, Léger R, Person V, Corn S, et al. Influence of hydrothermal ageing on the fatigue behaviour of a unidirectional flax-epoxy laminate. Compos Part B Eng 2019;174:107056.

[18] Jeannin T, Gabrion X, Ramasso E, Placet V. About the fatigue endurance of unidirectional flax-epoxy composite laminates. Compos Part B Eng 2019;165:690–701.

[19] Barbière R, Touchard F, Chocinski-Arnault L, Mellier D. Influence of moisture and drying on fatigue damage mechanisms in a woven hemp/epoxy composite: Acoustic emission and micro-CT analysis. Int J Fatigue 2020;136:105593.

[20] Xu Y, Wu Q, Lei Y, Yao F. Creep behavior of bagasse fiber reinforced polymer composites. Bioresour Technol 2010;101:3280–6.

[21] Saeed Kazemi Najafi, Sharifnia H, Tajvidi M. Effects of Water Absorption on Creep Behavior of Wood—Plastic Composites. J Compos Mater 2008;42:993–1002.

[22] Alvarez VA, Kenny JM, Vázquez A. Creep behavior of biocomposites based on sisal fiber reinforced cellulose derivatives/starch blends: Creep Behavior of Biocomposites. Polym Compos 2004;25:280–8.

[23] Yang T-C, Wu T-L, Hung K-C, Chen Y-L, Wu J-H. Mechanical properties and extended creep behavior of bamboo fiber reinforced recycled poly(lactic acid) composites using the time–temperature superposition principle. Constr Build Mater 2015;93:558–63.

[24] Tábi T, Bakonyi P, Hajba S, Herrera-Franco P, Czigány T, Kovács J. Creep behaviour of injection-moulded basalt fibre reinforced poly(lactic acid) composites. J Reinf Plast Compos 2016;35:1600–10.

[25] Poilâne C, Cherif ZE, Richard F, Vivet A, Ben Doudou B, Chen J. Polymer reinforced by flax fibres as a viscoelastoplastic material. Compos Struct 2014;112:100–12.

[26] Stochioiu C, Piezel B, Chettah A, Fontaine S, Gheorghiu H-M. Basic modeling of the visco elastic behavior of flax fiber composites. Ind Textila 2019;70:331–5.

[27] Morreale M, Mistretta M, Fiore V. Creep Behavior of Poly(lactic acid) Based Biocomposites. Materials 2017;10:395.

[28] Durante M, Formisano A, Boccarusso L, Langella A, Carrino L. Creep behaviour of polylactic acid reinforced by woven hemp fabric. Compos Part B Eng 2017;124:16–22.

[29] Abida M, Gehring F, Mars J, Vivet A, Dammak F, Haddar M. A viscoelastic–viscoplastic model with hygromechanical coupling for flax fibre reinforced polymer composites. Compos Sci Technol 2020;189:108018.

[30] Cisse O, Placet V, Guicheret-Retel V, Trivaudey F, Boubakar ML. Creep behaviour of single hemp fibres. Part I: viscoelastic properties and their scattering under constant climate. J Mater Sci 2015;50:1996–2006.

[31] Keryvin V, Lan M, Bourmaud A, Parenteau T, Charleux L, Baley C. Analysis of flax fibres viscoelastic behaviour at micro and nano scales. Compos Part Appl Sci Manuf 2015;68:219–25.

[32] Guicheret-Retel V, Cisse O, Placet V, Beaugrand J, Pernes M, Boubakar ML. Creep behaviour of single hemp fibres. Part II: Influence of loading level, moisture content and moisture variation. J Mater Sci 2015;50:2061–72.

[33] Boubakar ML, Vang L, Trivaudey F, Perreux D. A meso–macro finite element modelling of laminate structures. Compos Struct 2003;60:275–305.

[34] Corbin A-C, Soulat D, Ferreira M, Labanieh A-R, Gabrion X, Malécot P, et al. Towards hemp fabrics for high-performance composites: Influence of weave pattern and features. Compos Part B Eng 2020;181:107582.

[35] Test Methods for Constituent Content of Composite Materials. ASTM International; 2015

[36] Test Method for Moisture Absorption Properties and Equilibrium Conditioning of Polymer Matrix Composite Materials. ASTM International; 2012

[37] Test Method for Tensile Properties of Polymer Matrix Composite Materials. ASTM International; 2017

[38] Shah DU. Developing plant fibre composites for structural applications by optimising composite parameters: a critical review. J Mater Sci 2013;48:6083–107. https://doi.org/10.1007/s10853-013-7458-7.

[39] Plastics — Determination of creep behaviour — Part 1: Tensile creep. ISO; 2003

[40] Gottron J, Harries KA, Xu Q. Creep behaviour of bamboo. Constr Build Mater 2014;66:79–88.

[41] Ecotechnilin. Flaxtape Datasheet 2019.

[42] Placet V, Cissé O, Lamine Boubakar M. Nonlinear tensile behaviour of elementary hemp fibres. Part I: Investigation of the possible origins using repeated progressive loading with in situ microscopic observations. Compos Part Appl Sci Manuf 2014;56:319–27.

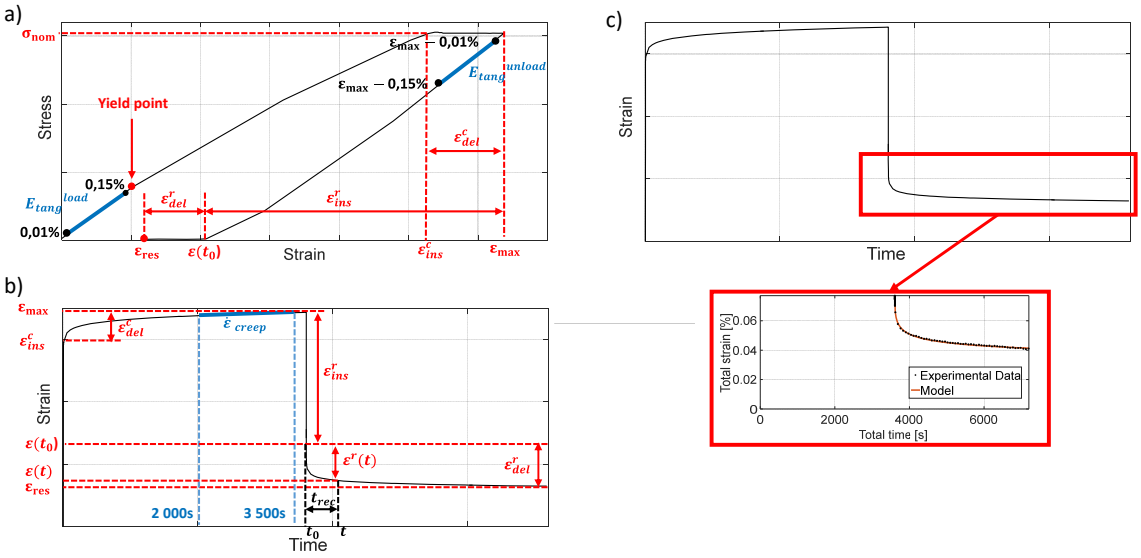

Fig. 1. Typical creep/recovery response plotted for stress-strain a) and strain-time b) diagrams and description of the recovery stage by the viscoelastic model c)

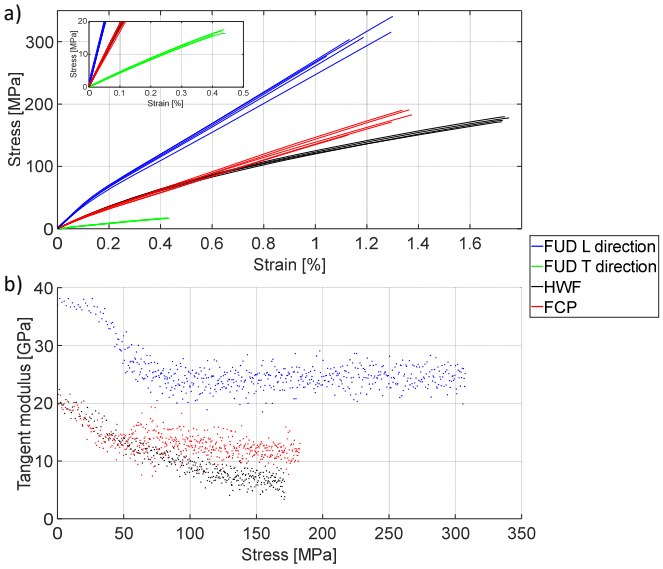

Fig. 2. Tensile stress-strain curves of the different composites a) and evolution of the tangent modulus as a function of the stress b) under environmental condition EC1

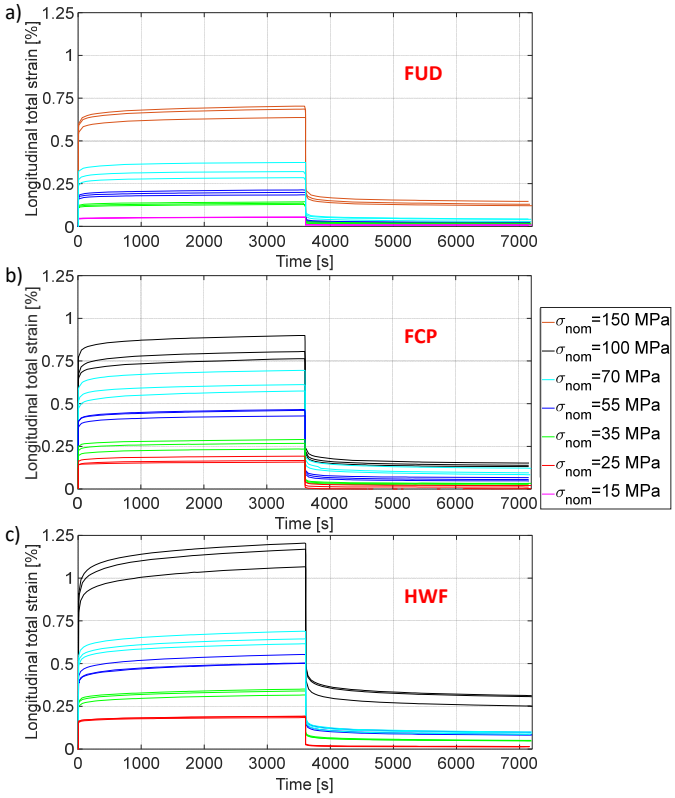

Fig. 3. Evolution of the total strain during a creep/recovery test on the FUD composite a), the FCP composite b) and the HWF composite c) for different stress levels under environmental condition EC1

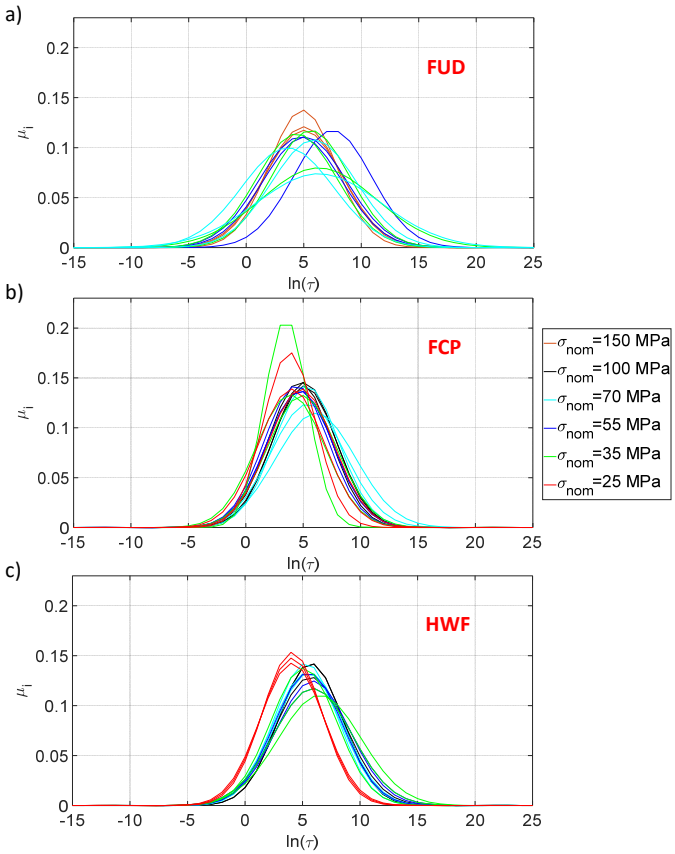

Fig. 4. Gaussian distribution of the weighting parameters as a function of the release time for each stress level identified from the recovery curve of the FUD composite a), FCP composite b) and HWF composite c)

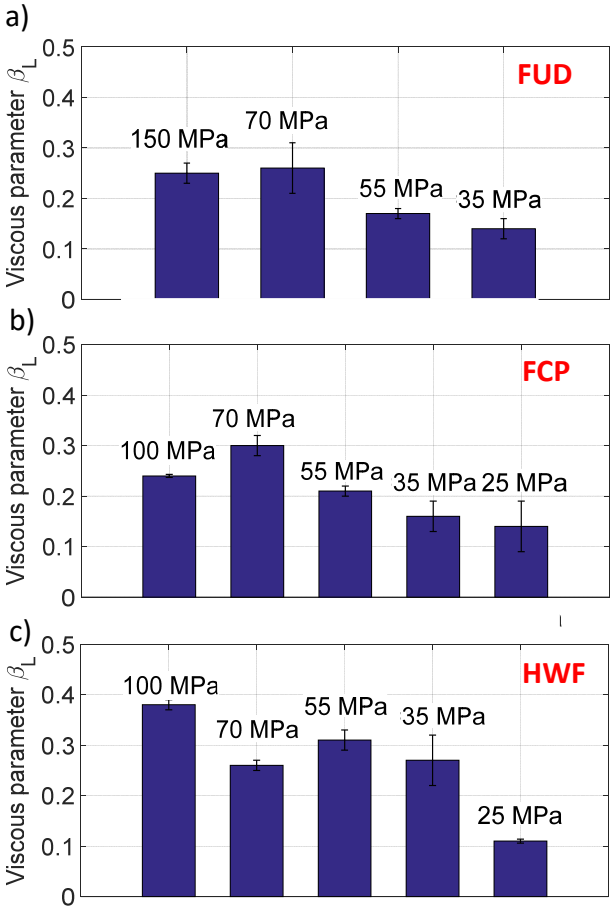

Fig. 5. Identified value of β_L depending on the stress level of each composite at environmental condition EC1

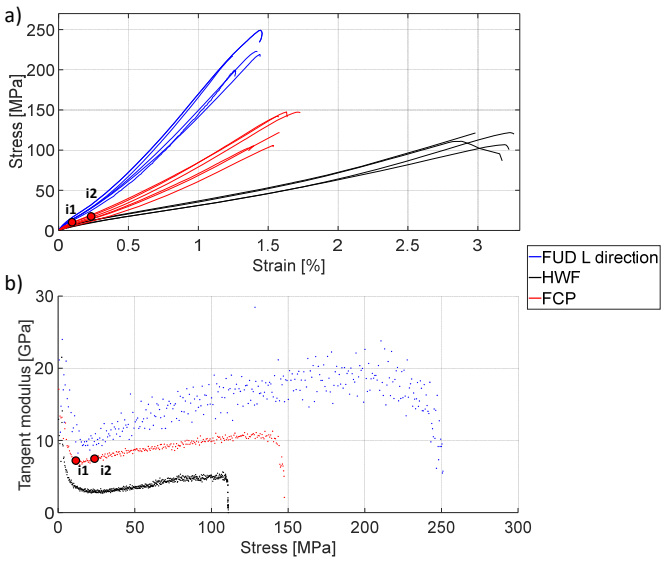

Fig. 6. Tensile stress-strain curves of the FUD, FCP and HWF composites a) and evolution of the apparent tangent modulus as a function of the stress b) under environmental condition EC2

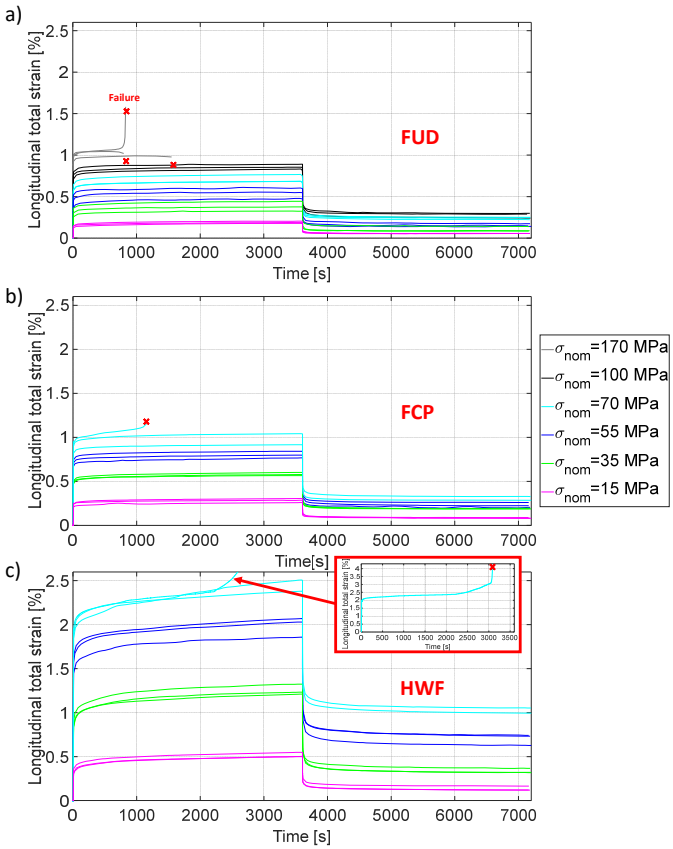

Fig. 7. Evolution of the total strain of the FUD composite a), the FCP composite b) and the HWF composite c) during a creep/recovery test under environmental condition EC2. The crosses represent the rupture of the specimen.

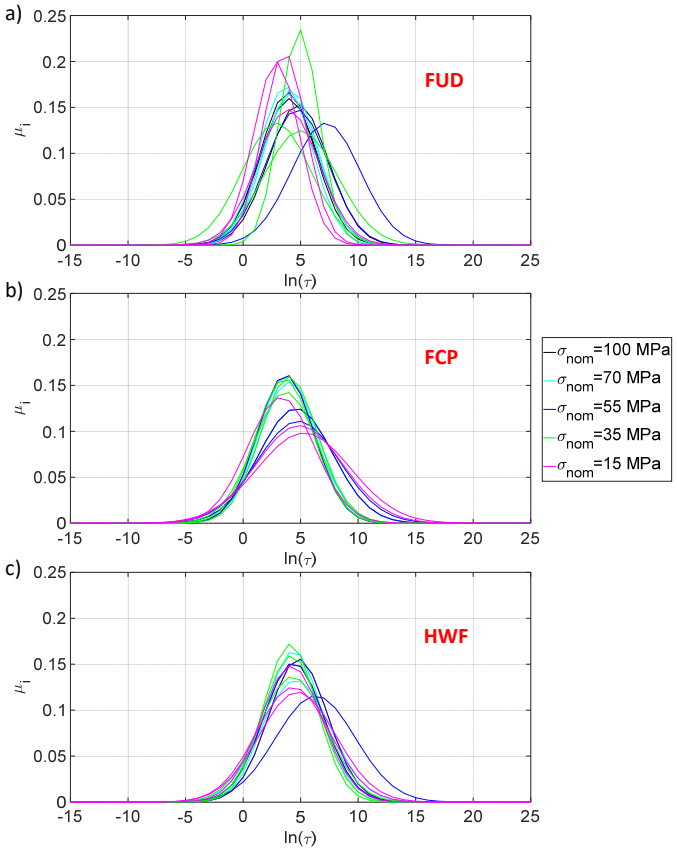

Fig. 8. Gaussian distribution of the weighting as a function of the release time obtained by the identification of the creep/recovery test carried out on the FUD composite a), FCP composite b) and HWF composite c) under environmental condition EC2

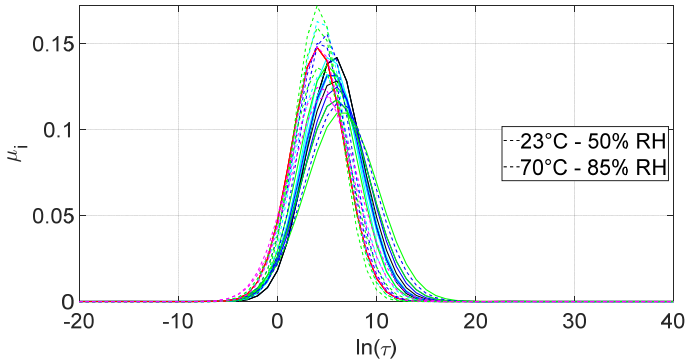

Fig. 9. Gaussian distribution of the weighting as a function of the release time obtained by the identification of the creep/recovery test carried out on the FUD composite at 23°C-50% RH and 70°C-85% RH

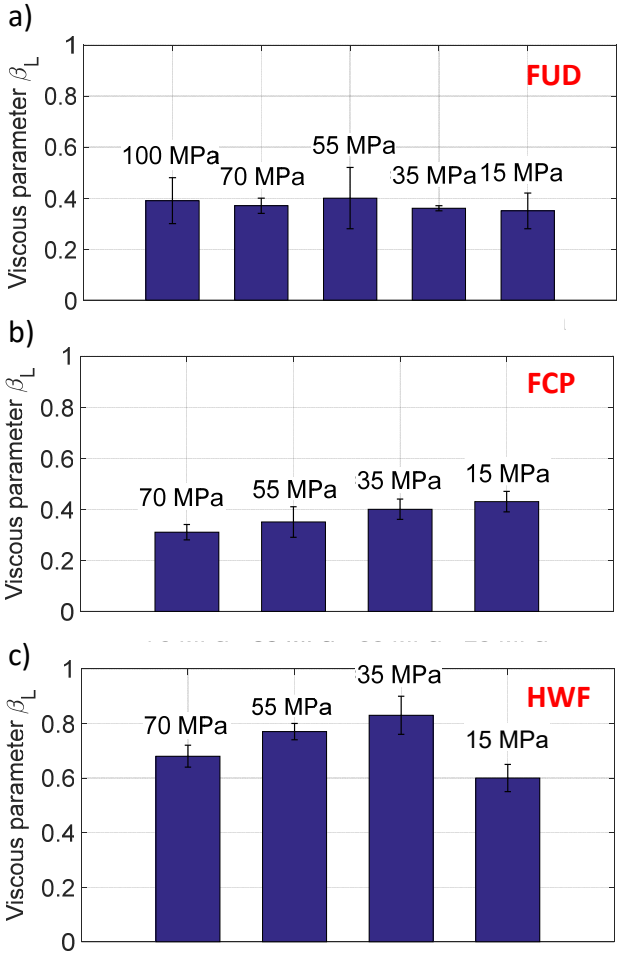

Fig. 10. Identified value of $\boldsymbol{\beta_L}$ depending on the stress level of each composite at environmental condition EC2

Tab. 1. Main features of the tested composite materials and samples

Reinforcement	Laminate	Sample orientation	Conditioning and testing environment	Stacking sequence	Dimensions of the samples (mm) (length x width x thickness)
FlaxTape	FUD	0° (L direction)	EC1	$[0]_{20}$	200x15x(2.92 ± 0.16)
			EC2	$[0]_{10}$	200x15x(1.58 ± 0.1)
		90° (T direction)	EC1	$[90]_{20}$	190x15x(2.92 ± 0.16)
			EC2		
	FCP	0°	EC1	$[(0/90)_{10}]_s$	190x15x(3.30 ± 0.05)
			EC2	$[(0/90)_4]_s$	190x15x(1.36 ± 0.03)
Hemp satin	HWF	Weft	EC1	$[0]_4$	195x15x(1.95 ± 0.08)
			EC2		

Tab. 2. Fabrication parameters for the three types of composites (mean value ± standard deviation)

Composite	Tc [°C]	Tpc [°C]	dpc [h]	Tpr [°C]	Vf [%]	Vv [%]	$M_{C\infty}1$ [%]	$M_{C\infty}2$ [%]
FUD	80	80	2	80	51 ± 1	2 ± 1	3.3 ± 0.1	8.9 ± 0.1
FCP	60	130	1	30	44 ± 1	2 ± 2	3.8 ± 0.2	8.8 ± 0.3
HWF	60	130	1	30	48 ± 2	1 ± 2	3.2 ± 0.2	8.6 ± 0.2

Tab. 3. Properties in each material direction obtained under monotonic tensile tests up to failure for each type of composite under each environmental condition (mean value ± standard deviation)

Environmental condition	Composite	Material direction	E_L^1 [GPa]	E_L^2 [GPa]	E_T [GPa]	Stress at failure [MPa]	Strain at failure [%]
EC1	FUD	L	36 ± 2	24 ± 1	-	311 ± 21	1.18 ± 0.10
		T	-	-	4.2 ± 0.1	16 ± 2	0.38 ±0.04
	FCP	-	17 ± 1	13 ± 1	-	177 ± 17	1.30 ± 0.10
	HWF	-	19 ± 1	-	-	176 ± 3	1.74 ± 0.01
EC2	FUD	L	13 ± 1	-	-	227 ± 20	1.43 ± 0.17
	FCP	-	7 ± 2	-	-	128 ± 20	1.59 ± 0.09
	HWF	-	5 ± 1	-	-	117 ± 8	3.11 ± 0.14

Tab. 4. Values of the stiffening coefficient, secondary creep strain rate, instantaneous strain, time-delayed strain, maximum strain and residual strain extracted from the creep/recovery test on the FUD composite at environmental condition EC1 for each stress level (mean value ± standard deviation)

	15 MPa	35 MPa	55 MPa	70 MPa	150 MPa
S [%]	0	0	0	1.4 ± 1.0	9.9 ± 0.6
$\dot{\varepsilon}_{creep}$ [10^{-8} s^{-1}]	0.5 ± 0.1	2.3 ± 0.3	2.1 ± 0.4	1.8 ± 0.3	6.3 ± 0.7
ε_{ins}^{c}[%]	0.044 ± 0.002	0.11 ± 0.01	0.16 ± 0.01	0.27 ± 0.04	0.56 ± 0.03
ε_{ins}^{r}[%]	0.043 ± 0.002	0.11 ± 0.01	0.16 ± 0.01	0.25 ± 0.04	0.45 ± 0.02
ε_{del}^{c} [%]	0.009 ± 0.001	0.022 ± 0.001	0.039 ± 0.002	0.058 ± 0.004	0.116 ± 0.010
ε_{del}^{r} [%]	0.003 ± 0.001	0.012 ± 0.001	0.022± 0.004	0.040 ± 0.005	0.092 ± 0.003
ε_{max} [%]	0.054 ± 0.001	0.14 ± 0.01	0.20 ± 0.02	0.33 ± 0.04	0.68 ± 0.03
ε_{res} [%]	0.008 ± 0.002	0.016 ± 0.003	0.020 ± 0.004	0.037 ± 0.008	0.13 ± 0.02

Tab. 5. Values of the stiffening coefficient, secondary creep strain rate, instantaneous strain, time-delayed strain, maximum strain and residual strain extracted from the creep/recovery test on the FCP composite at environmental condition EC1 for each stress level (mean value ± standard deviation)

	25 MPa	**35 MPa**	**55 MPa**	**70 MPa**	**100 MPa**
S [%]	0	0	2.8 ± 1.3	7.6 ± 2.4	6.5 ± 7.5
$\dot{\varepsilon}_{creep}$ **[10^{-8} s^{-1}]**	2.11 ± 0.2	3.0 ± 0.5	4.9 ± 1.1	6.6 ± 0.5	8.6 ± 1.0
ε_{ins}^{c}**[%]**	0.14 ± 0.01	0.22 ± 0.03	0.37 ± 0.02	0.50 ± 0.06	0.67 ± 0.06
ε_{ins}^{r}**[%]**	0.14 ± 0.01	0.21 ± 0.03	0.34 ± 0.01	0.44 ± 0.05	0.58 ± 0.05
ε_{del}^{c} **[%]**	0.028 ± 0.009	0.050 ± 0.003	0.08 ± 0.01	0.13 ± 0.01	0.16 ± 0.01
ε_{del}^{r} **[%]**	0.018 ± 0.006	0.0290 ± 0.0004	0.055 ± 0.003	0.09 ± 0.01	0.10 ± 0.01
ε_{max} **[%]**	0.17 ± 0.02	0.26 ± 0.03	0.45 ± 0.02	0.63 ± 0.06	0.82 ± 0.07
ε_{res} **[%]**	0.011 ± 0.009	0.030 ± 0.004	0.06 ± 0.01	0.10 ± 0.01	0.14 ± 0.01

Tab. 6. Values of the stiffening coefficient, secondary creep strain rate, instantaneous strain, time-delayed strain, maximum strain and residual strain extracted from the creep/recovery test on the HWF composite at environmental condition EC1 for each stress level (mean value ± standard deviation)

	25 MPa	**35 MPa**	**55 MPa**	**70 MPa**	**100 MPa**
S [%]	0	0	0.7 ± 1.0	4.3 ± 0.6	6.4 ± 4.0
$\dot{\varepsilon}_{creep}$ **[10^{-8} s^{-1}]**	2.64 ± 0.8	6.1 ± 0.7	9.4 ± 0.8	10.3 ± 1.1	19.2 ± 0.9
ε_{ins}^{c}**[%]**	0.157 ± 0.003	0.25 ± 0.02	0.39 ± 0.02	0.50 ± 0.03	0.82 ± 0.05
ε_{ins}^{r}**[%]**	0.159 ± 0.006	0.24 ± 0.02	0.35 ± 0.02	0.47 ± 0.03	0.68 ± 0.03
ε_{del}^{c} **[%]**	0.032 ± 0.002	0.081 ± 0.002	0.13 ± 0.001	0.15 ± 0.01	0.33 ± 0.03
ε_{del}^{r} **[%]**	0.017 ± 0.001	0.047 ± 0.001	0.078 ± 0.005	0.086 ± 0.003	0.173 ± 0.005
ε_{max} **[%]**	0.19 ± 0.01	0.34 ± 0.02	0.52 ± 0.03	0.65 ± 0.04	1.15 ± 0.07
ε_{res} **[%]**	0.014 ± 0.001	0.049 ± 0.002	0.09 ± 0.01	0.09 ± 0.01	0.29 ± 0.03

Tab. 7. Values of the model parameters after identification of the recovery stage of the composites for each environmental condition (mean value ± standard deviation)

Environmental Condition	Composite	$\ln(\tau_1)$	SD	$\frac{\beta_L}{E_L}$ [MPa^{-1}]
EC1	FUD	5.6 ± 0.9	3.8 ± 0.7	6.1 .10^{-6} ± 2.1 .10^{-6}
	FCP	5.0 ± 1.3	3.0 ± 0.6	1.2 .10^{-5} ± 4.4 .10^{-6}
	HWF	5.4 ± 0.7	3.0 ± 0.3	1.5 .10^{-5} ± 4.9 .10^{-6}
EC2	FUD	4.3 ± 1.0	2.3 ± 0.6	1.6 .10^{-5} ± 4.3 .10^{-6}
	FCP	4.1 ± 0.6	3.0 ± 0.6	2.7 .10^{-5} ± 1.3 .10^{-5}
	HWF	4.6 ± 0.6	2.8 ± 0.4	7.0 .10^{-5} ± 1.4 .10^{-5}

Tab. 8. Values of the stiffening coefficient, secondary creep strain rate, instantaneous strain, time-delayed strain, maximum strain and residual strain extracted from the creep/recovery test on the FUD composite at environmental condition EC2 for each stress level (mean value ± standard deviation)

	15 MPa	35 MPa	55 MPa	70 MPa	100 MPa	170 MPa
S [%]	18 ± 5	47 ± 13	52 ± 8	73 ± 10	100 ± 18	-
$\dot{\varepsilon}_{creep}$ [10^{-8} s^{-1}]	3.6 ± 0.9	4.2 ± 1.9	5.4 ± 2.8	6.0 ± 0.6	4.6 ± 3.8	-
ε_{ins}^{c}[%]	0.14 ± 0.05	0.27 ± 0.05	0.39 ± 0.07	0.55 ± 0.01	0.81 ± 0.15	0.94 ± 0.05
ε_{ins}^{r}[%]	0.10 ± 0.01	0.24 ± 0.06	0.34 ± 0.04	0.38 ± 0.04	0.47 ± 0.02	-
ε_{del}^{c} [%]	0.08 ± 0.01	0.11 ± 0.01	0.16 ± 0.01	0.16 ± 0.04	0.18 ± 0.06	-
ε_{del}^{r} [%]	0.03 ± 0.01	0.06 ± 0.01	0.06 ± 0.01	0.10 ± 0.01	0.12 ± 0.02	
ε_{max} [%]	0.19 ± 0.01	0.38 ± 0.06	0.55 ± 0.07	0.71 ± 0.05	0.86 ± 0.03	1.20 ± 0.33
ε_{res} [%]	0.055 ± 0.002	0.10 ± 0.03	0.15 ± 0.02	0.24 ± 0.02	0.28 ± 0.03	-

Tab. 9. Values of the stiffening coefficient, secondary creep strain rate, instantaneous strain, time-delayed strain, maximum strain and residual strain extracted from the creep/recovery test on the FCP composite at environmental condition EC2 for each stress level (mean value ± standard deviation)

	15 MPa	**35 MPa**	**55 MPa**	**70 MPa**
S [%]	45 ± 2	64 ± 4	91 ± 18	94 ± 1
$\dot{\varepsilon}_{creep}$ **[10^{-8} s^{-1}]**	3.6 ± 1.1	6.6 ± 0.8	6.8 ± 2.2	5.4 ± 1.2
ε_{ins}^{c}**[%]**	0.16 ± 0.04	0.46 ± 0.01	0.68 ± 0.03	0.85 ± 0.06
ε_{ins}^{r}**[%]**	0.14 ± 0.01	0.31 ± 0.01	0.47 ± 0.01	0.56 ± 0.04
ε_{del}^{c} **[%]**	0.06 ± 0.03	0.10 ± 0.02	0.12 ± 0.01	0.15 ± 0.03
ε_{del}^{r} **[%]**	0.06 ± 0.02	0.09 ± 0.01	0.11 ± 0.01	0.11 ± 0.02
ε_{max} **[%]**	0.29 ± 0.02	0.58 ± 0.02	0.8 ± 0.04	1.04 ± 0.12
ε_{res} **[%]**	0.08 ± 0.01	0.19 ± 0.01	0.23 ± 0.03	0.31 ± 0.03

Tab. 10. Values of the stiffening coefficient, secondary creep strain rate, instantaneous strain, time-delayed strain, maximum strain and residual strain extracted from the creep/recovery test on the HWF composite at environmental condition EC2 for each stress level (mean value ± standard deviation)

	15 MPa	**35 MPa**	**55 MPa**	**70 MPa**
S [%]	1 ± 1	27 ± 2	68 ± 18	72 ± 9
$\dot{\varepsilon}_{creep}$ **[10^{-8} s^{-1}]**	14.6 ± 1.6	22.4 ± 2.8	32.9 ± 10.7	62.9 ± 31.3
ε_{ins}^{c}**[%]**	0.27 ± 0.02	0.74 ± 0.03	1.38 ± 0.10	1.71 ± 0.06
ε_{ins}^{r}**[%]**	0.27 ± 0.01	0.66 ± 0.05	0.99 ± 0.05	1.10 ± 0.05
ε_{del}^{c} **[%]**	0.24 ± 0.01	0.51 ± 0.03	0.61 ± 0.02	0.76 ± 0.13
ε_{del}^{r} **[%]**	0.11 ± 0.05	0.26 ± 0.02	0.29 ± 0.03	0.329 ± 0.002
ε_{max} **[%]**	0.52 ± 0.03	1.25 ± 0.06	1.99 ± 0.11	2.97 ± 0.91
ε_{res} **[%]**	0.13 ± 0.03	0.33 ± 0.03	0.70 ± 0.06	1.02 ± 0.04

List of figures

List of tables